CrossMark

RESEARCH ARTICLE

# Voronoï analysis of bubbly flows via ultrafast X-ray tomographic imaging

Yuk Man Lau[1] · Karolin Müller[1] · Salar Azizi[1] · Markus Schubert[1]

**Abstract** Although clustering of bubbles plays a significant role in bubble column reactors regarding the heat and mass transfer due to bubble–bubble and flow field interactions, it has yet to be fully understood. Contrary to flows in bubble columns, most literature studies on clustering report numerical and experimental results on dilute or micro-bubbly flows. In this paper, clustering of bubbles in a cylindrical bubble column of 100 mm diameter is experimentally investigated. Ultrafast X-ray tomographic imaging is used to obtain the bubble positions within a hybrid Eulerian framework. By means of Voronoï analysis, the clustering behavior of bubbles is investigated. Experiments are performed with different superficial gas velocities, where Voronoï diagrams are constructed at several column heights. From the PDFs of the Voronoï diagrams, it is shown that the bubble structuring in terms of Voronoï cell volumes develops slower than the bubble size distribution. The latter reaches a steady state earlier with increasing column height. The measured PDFs are compared with the PDF of randomly distributed points, which showed that the amount of bubbles as part of clusters (Voronoï cells $< V/\overline{V}_{\text{cluster}}$) as well as bubbles as part of voids (Voronoï cells $> V/\overline{V}_{\text{void}}$) increases with the superficial gas velocity. It is found that all experiments have an approximate cluster limit $V/\overline{V}_{\text{cluster}}$ of 0.63, while the void limit $V/\overline{V}_{\text{void}}$ varies between 1.5 and 3.0.

✉ Markus Schubert
m.schubert@hzdr.de

Yuk Man Lau
y.m.lau@hzdr.de

[1]   Institute of Fluid Dynamics, Helmholtz-Zentrum Dresden-Rossendorf e.V., Bautzner Landstrasse 400, 01328 Dresden, Germany

## 1 Introduction

Already in the 1990s, numerical simulations were performed for examining the behavior of bubble swarms and allowed first qualitative conclusions on, for instance, bubble alignments. Sangani and Didwania (1993) focused on rising bubbles of high Reynolds number and found the homogeneous state of the system to be unstable. The initially uniformly distributed bubbles tend to cluster perpendicular to the flow direction. Different scenarios were investigated such as simulations with or without viscous forces. From these simulations, they discovered that viscous forces play an important role in facilitating aggregate formations. While the authors could not observe clustering by neglecting the viscous forces and applying a broad initial velocity distribution simultaneously, they detected that bubbles aggregate for any form of the bubble velocity distribution in cases, where the viscous forces were taken into account. Smereka (1993) found similar results for the viscous simulations with different bubble size and velocity distributions. For inviscid bubbly flows, clustering only occurs, if the initial velocity distribution is uniform. Contrarily, for non-uniform initial velocity distribution or large variance of velocities, no clusters are formed. Smereka (1993) viewed the variance of the bubble velocities as the effect of temperature on clustering. According to his study, the increase in temperature hinders the bubble alignment. Similar results were obtained from other numerical studies (Bunner and Tryggvason 2002; Mazzitelli and Lohse 2009; Santarelli and Fröhlich 2013), but also proven by experiments such as the work of Zenit et al. (2001). They concluded clustering by means of velocity variance and verified it by analyzing video images. However, they found far weaker clustering in their experiments than expected from earlier stated numerical results. Mazzitelli and Lohse

 Springer

(2009) noted from simulations that in the wake of a rising bubble the appearing lift force affects successive bubbles. As a result the following bubbles are forced to move sideward so that they start to align horizontally since the formation of vertical clusters does not occur or arises fairly unstable. Similar phenomena were found in the experiments by Koch (1993), who attributed the deficit of bubbles in the wake of other bubbles to the lift force. Esmaeeli and Tryggvason (1998, 1999) employed direct numerical simulations to investigate arrays of bubbles for small and high Reynolds numbers. They noticed that a regular array rises much slower than irregular ones. By starting with an initial regular array, after the rising bubbles reach the wake of the bubbles in front, the array becomes unstable and the initial configuration breaks up, which results in an irregular array. Bunner and Tryggvason (2002) employed the pair correlation function to computationally study the structuring of bubbles, which revealed a preference for pairs of bubbles to be aligned horizontally. Although this is consistent with potential flow theory, the dynamics of bubble–bubble interactions within the simulations are significantly different from potential flow predictions. In steady potential flow, two spheres attract, when they move perpendicularly to their line of centers and repel, when they move in the direction parallel to their line of centers (Lamb 1932). Contrarily, in the simulations of Bunner and Tryggvason (2002), two vertically aligned bubbles attract each other due to the wake effect, rotate around each other and then repel, when they are aligned horizontally. These dynamics are caused by the wake effect and the pressure in between the bubble gap and are also called: drafting, kissing and tumbling. Bunner and Tryggvason (2003) showed that the deformability of the bubble shapes changes the clustering structure, where spherical bubbles cluster horizontally, while ellipsoidal bubbles preferably align vertically. Simulations of bubble swarms by Smolianski et al. (2008) with ellipsoidally and spherically shaped bubbles confirmed the dependence of the swarm dynamics on the liquid's Morton number Mo ($=$Eö$^3$/$Re^4$). At low Morton numbers, there is increased clustering leading to coalescence in bubble swarms and thus creating larger bubbles, while at high Morton numbers coalescence has not been observed and therefore fosters a larger interfacial area, which is more advantageous regarding mass transfer. This is in accordance with the experimental study of Risso and Ellingsen (2002), who examined rising bubbles bearing a high Reynolds number and could not observe any cluster formation. It should be noted that, since the Morton number is inversely proportional to the fourth power of the Reynolds number, there is some trade-off between a large interfacial area and high Reynolds numbers for individual bubbles. Ferreira et al. (2008) studied the complexity of bubble swarms in bubble columns in relation to the superficial gas velocity and the sparger orifice diameter by means of image analysis. They found that the complexity of bubble swarms increases with increasing superficial gas velocity and a reduced mass transfer coefficient occurred with the presence of bubble clusters. The mass transfer is reduced, because the concentration of the dissolved gas in the liquid around a single gas bubble in a swarm depends not only on the mass transfer from the bubble itself, but also on the mass transfer from the other bubbles in the swarm.

Besides swarms in bubble columns, clustering is worth to be studied with regard to several other applications as well. Amongst others regarding flotation processes, e.g., Yianatos et al. (1988) adapted a beforehand for particles developed formula for hindered settling to bubbles and estimated the bubble size in a swarm. Their formula provides a good approximation for low Reynolds numbers so that it was well applicable for flotation. To characterize individual bubbles, such as size and velocity, within clusters, Acuña and Finch (2010) used digital image analysis on the flotation process in a pseudo-2D bubble column. This experimental technique is not suitable to investigate three-dimensional bubbly flows, and advanced methods are required.

From the above mentioned studies, it can be concluded that investigations of clustering in bubbly flows are performed either using simulations or with experiments of dilute bubbly flow. Although clustering in bubble column reactors plays a major role in heat and mass transfer, it has yet to be studied in-depth. In this paper, the clustering of bubbles in bubble columns is investigated by means of Voronoï analysis on ultrafast X-ray tomography data. The Voronoï analysis is a powerful technique, which can give detailed information about clustering. Compared with other methods to describe local concentration fields, such as the box counting method (Aliseda et al. 2002), which is computationally inefficient and requires a selected arbitrary length scale (the box size), for Voronoï diagrams computation no length scale is a priori chosen and the resulting local concentration field is obtained at an intrinsic resolution. Similarly, the pair correlation function (Martinez Mercado et al. 2010), which only provides global (non-local) information, also requires a choice of a length scale of interest, which is proportionally coupled with the computation time. Another interesting use of Voronoï diagrams (Monchaux et al. 2010; Martinez Mercado et al. 2012; Tagawa et al. 2012) is that since each individual cell is associated with a given bubble at each time step, tracking the bubbles in a Lagrangian framework provides insights into the dynamics of the concentration field along the bubble trajectories. Contrary to the abovementioned Voronoï studies, in the current context Voronoï diagrams are applied within an Eulerian framework to investigate clustering in a bubble column. In such

**Fig. 1** Methodology: **a** Ultrafast X-ray tomographic images of 240 × 240 pixels are stacked in a time frame of 1 s (1000 images) to provide a three-dimensional phase fraction field; **b** from the Eulerian field, the centroids of the bubble objects are extracted; and **c** used as input to create a Voronoï diagram for further analysis



**(a)** X-ray data                    **(b)** Bubble centroids                    **(c)** 3D Voronoï diagram
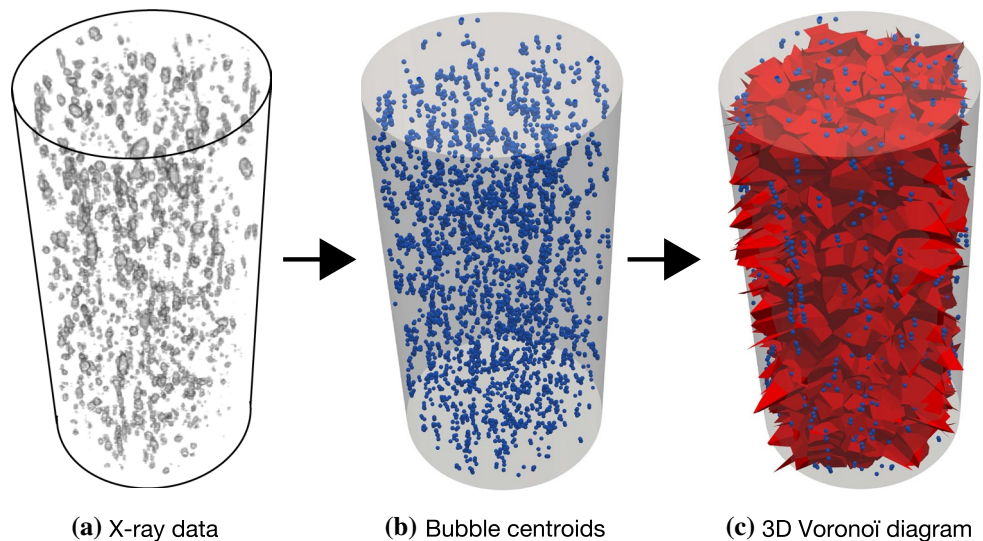
framework, instead of tracking the bubble trajectories, the bubbles in terms of the phase fraction images are measured at a fixed plane, which is the X-ray scanning plane. By stacking these images in time, a hybrid three-dimensional field of bubbles is obtained. Using the centroids of the bubbles, a Voronoï diagram is created for further analysis. A brief overview of this method is given in Fig. 1. Voronoï analysis is chosen based on an evaluation of the methods used in previous literature, from which we concluded that Voronoï diagrams are best suited for the current framework. The main advantage of this method is, that compared with others, for instance the box counting method, there is no need for an arbitrarily chosen length scale.

This paper is structured as follows. First, a description of the experimental setup is given, respectively, the ultrafast X-ray tomograph setup and the bubble column. Subsequently, the method of Voronoï diagrams applied to the acquired X-ray data is explained. With this method, the clustering behavior of bubbles in a cylindrical bubble column is investigated. Finally, conclusions regarding the results, for instance the effect of superficial gas velocity on clusters, are given. Such findings provide insight on the impact of clusters on the process performance of the bubble column, where the formation of clusters affects the heat and mass transfer.

## 2 Experiments

### 2.1 Ultrafast X-ray tomography

In this study, the experimental data used for examining bubble clustering are obtained using ultrafast X-ray computerized tomography (CT). This measurement technique
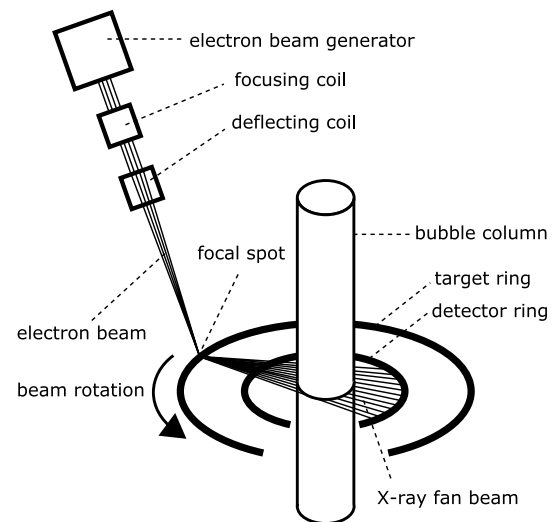


**Fig. 2** Novel ultrafast X-ray tomographic scanner

is developed by Fischer et al. (2008) and has the ability to achieve a measurement frequency of up to 8000 Hz with a spatial resolution of approximately 1 mm. The advantage of the X-ray CT principle is its non-intrusive nature. X-rays are able to penetrate wall materials, so that the intrinsic hydrodynamics inside the process, namely the gas–liquid flow within the bubble column, is not affected during sampling. Transparent material, as required for video treatment, is not necessary. With this technique, it is feasible to visualize dense bubbly flows that are not accessible with optical techniques. The experimental tomography setup (Fig. 2 for schematics) consists of an electron beam gun, a system of coils (beam optics) for beam modification and the X-ray target and detector rings. The electron beam itself is
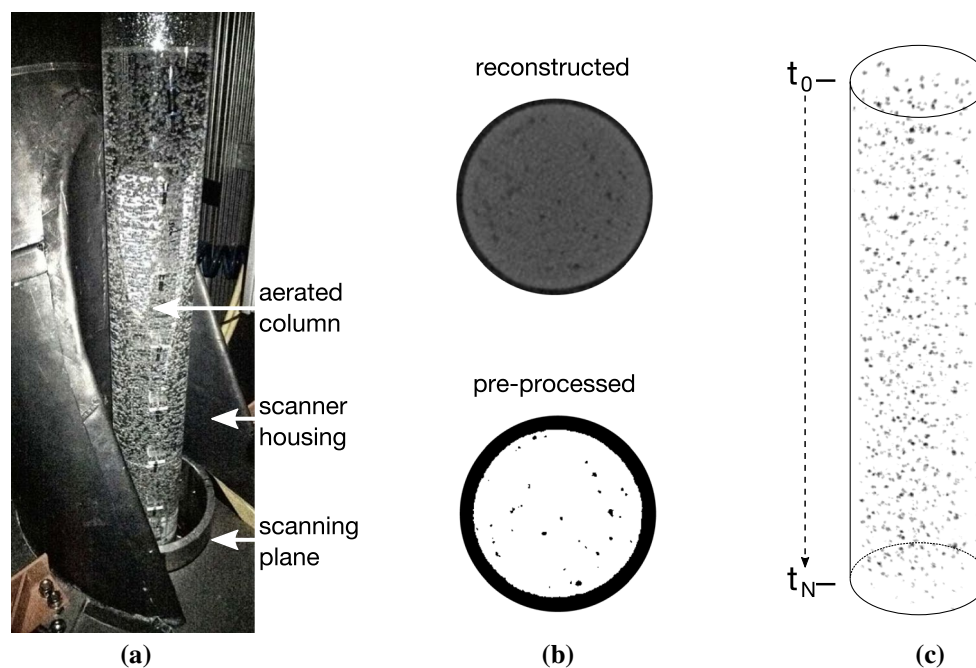
**Fig. 3** Experimental setup and resulting data: **a** bubble column; **b** reconstructed images at a certain time step; and **c** thresholded X-ray images stacked over time

generated by means of a high voltage generator. An operation rack to fix the scanner and to adjust the scanned objects as well as a measurement PC for data processing completes the system. It should be noted that the current equipment is a newly constructed scanner with increased capacity of measurement geometry up to column diameters of 160 mm in contrary to the previous scanner (Fischer et al. 2008; Fischer and Hampel 2010; Hampel et al. 2012). The maximum operating frequency is 8000 Hz, which is similar to the older scanner. To achieve this increased capacity, the target and detector rings are enlarged. The detector ring consists of 423 elements compared with 240 elements of the older setup. This translates to an increase in image resolutions to $240 \times 240$ pixels compared with $120 \times 120$ of the older setup. The spatial accuracy is approximately 1 mm. The working principle (Fig. 2) and data processing remain the same as described in earlier literature. Basically, the focus of the generated electron beam is guided along the path of the Tungsten target ring, producing a moving X-ray source rotating around the object of measurement. This is the main difference to conventional systems, which rely on mechanical rotations to acquire 360° recordings. Without moving parts, ultrafast X-ray tomography can reach high measurement frequencies using only beam deflections. The signals of the generated X-ray fan beam from the focal spot are recorded within the detector ring, and the cross-sectional images are reconstructed from the obtained tomographic data using the filtered back-projection method.

## 2.2 Bubble column

The laboratory bubble column is an air–water system and is shown in Fig. 3a. The column wall is constructed from acrylic glass and has a diameter of 100 mm with a height of 1 m and a wall thickness of 5 mm. The initial liquid height is set at 0.70 m. Gas is dispersed in the bubble column via a needle sparger, which consists of 115 needles with an inner diameter of 0.22 mm, an outer diameter of 0.40 mm and a length of 40 mm. In comparison with a porous plate, the use of a needle sparger produces a narrow bubble size distribution with low bubble diameter. The X-ray scanner is operated with an imaging frequency of 1000 Hz for a measurement time of 10 s. As mentioned earlier, the images are reconstructed using the filtered back-projection method. Subsequently, the raw images are preprocessed. First, the solid column wall is subtracted from the images. From the measured empty and liquid-filled column X-ray data, the images are normalized by setting 0 for the gas phase and 1 for the liquid phase. Hereafter, the images are segmented with a threshold of 0.6, which has been obtained through verification with phantom measurements. Figure 3b illustrates the raw constructed and the preprocessed images. The preprocessed images are stacked in the time domain to obtain three-dimensional bubble objects with hybrid dimensions of time and space (Fig. 3c). The centroids of these bubbles are used for the construction of Voronoï diagrams.

# 3 Voronoï analysis

## 3.1 Voronoï diagrams and clustering

A Voronoï diagram is a spatial tessellation (Okabe et al. 2000), where each Voronoï cell is defined at the bubble location based on the distance to the neighboring bubbles. Examples of Voronoï diagrams in 2D and 3D are shown in Fig. 4. Every point in a Voronoï cell is closest to the bubble position compared with the neighboring bubbles excluding the vertices, borderlines and facets (only in 3D). Therefore, in regions where bubbles cluster, the area (2D) or volume (3D) of the Voronoï cells is smaller than that of the cells in the neighboring regions. Hence, the area (2D) or volume (3D) of the Voronoï cells is inversely proportional to the local bubble concentration. For randomly distributed bubbles, since there is no analytical solution available, the probability density function (PDF) of the Voronoï areas/volumes normalized by the mean value is usually described with a $\Gamma$-distribution (Monchaux et al. 2010). Ferenc and Néda (2007) provided an approximation for the three-dimensional case of the random PDF using the following equation:

$$f(x) = \frac{3125}{24}x^4 \exp(-5x) \tag{1}$$

with $f$ the probability and $x$ the Voronoï cell volume. Similar to the box counting method, the measured PDF of the Voronoï cells is compared with the random PDF. Bubbles, which are not randomly distributed, will have a PDF that deviates from the random distribution, indicating a larger emphasis on the presence of clusters as well as voids.

In the presence of clustering, the probability of finding Voronoï cells with the mean area/volume size decreases, whereas the detection of very large and very small cells in turn is more probable. To identify Voronoï cells and, indirectly the individual bubbles as part of clusters or voids, a similar technique of PDF analysis as given by Monchaux et al. (2010) can be applied. Using this procedure, regions with high and small bubble concentrations can be revealed. These regions, albeit easier in 2D than in 3D analysis, can be visualized in Voronoï diagrams via dyeing or coloring of cells, so that information about cluster and void morphology, respectively, may be provided. For that purpose the intersection points between the measured and the random PDF as limits for cluster and void definition are taken into account (Monchaux et al. 2010, 2012).

## 3.2 Experimental Voronoï diagrams

### 3.2.1 Hybrid dimensions

The application of the current Voronoï analysis differs from previous literature studies, whereas the cluster analysis is performed on a two- or three-dimensional spatial framework. Here, the obtained X-ray data have hybrid dimensions, respectively, two spatial dimensions in the scanning plane and a third temporal dimension due to stacking. This stacking in time can be viewed as freezing the bubbles in time once they pass the scanning or measurement plane. Since analysis of passing bubbles is performed at a fixed location, Eulerian statistics can be acquired. Instead of Lagrangian statistics, where the bubbles are followed in time, in the current context the Voronoï cells are constructed on the basis of how much two-dimensional space a bubble occupies in time as it passes the scanning plane. Thus, this creates hybrid-dimensional Voronoï cells of the bubbly flow. Since time is a relative dimension in the X-ray data, an averaged bubble velocity is used to convert the time to a quasi-spatial dimension. The averaged bubble velocity is based on the superficial gas velocity divided by the time-averaged local gas hold-up. This temporal–spatial conversion can be seen as a scaling of the size of the hybrid Voronoï cells.
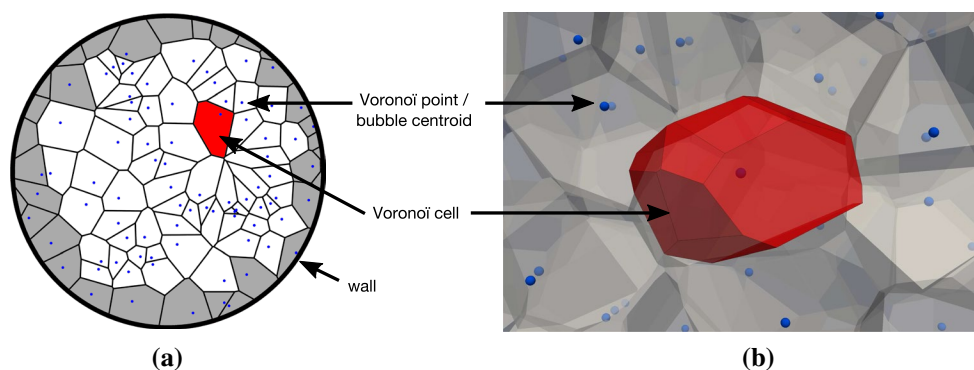


**Fig. 4** Examples of Voronoï diagrams of randomly generated bubble centroids, which are *blue-colored* and a highlighted *red-colored* Voronoï cell in: (**a**) 2D with *white-colored* bulk and *gray-colored* boundary cells; and (**b**) 3D

### 3.2.2 Neglecting bubble size and boundary cells

For the construction of the Voronoï diagrams of the experimental data, the centroids of the bubbles are considered as the Voronoï points. The different bubble sizes are neglected for the current investigation. To minimize the effect of different bubble sizes, experiments are performed with the bubble column operating at low superficial gas velocities and by using a sparger with a large number of needles, of which the injected bubbles are more uniformly sized in comparison with a porous plate. Another assumption in the construction of the experimental Voronoï diagrams is to discard wall boundary cells (illustrated as gray-colored cells in Fig. 4a), since clustering in the bulk of the bubble column is of main interest. Although not all wall cells are ill-defined (infinite volume due to the construction of the Voronoï diagram), the volume of these cells is affected by the cutoff of the column wall.

## 4 Results and discussion

Experiments of the bubble column have been performed using low superficial gas velocities $v_{sup} = 1.06$, $3.18$ and $5.31$ cm/s with their measured time-averaged void fractions of 0.01, 0.06 and 0.07. The measurements with ultrafast X-ray tomography are taken at several heights $h = 1$, 10, 30 and 50 cm.

### 4.1 Bubble size distribution

The PDFs of the measured bubble size distributions are illustrated in Fig. 5. The bubble size distributions are approximated using the averaged bubble velocity times the occupied voxels of each bubble object in the hybrid three-dimensional phase fraction field (Fig. 1a):

$$V_{bubble} = \left( \sum_{bubble} voxels \right) \cdot dx \cdot dy \cdot (\overline{v}_{bubble} \cdot dt) \quad (2)$$

where the bubble volume $V_{bubble}$ is the sum of voxels belonging to the identified three-dimensional ($x$, $y$ and $z$) bubble object in the hybrid-dimensional framework. Each voxel has the dimensions of $px^2 \cdot s$. The dimensions of the $x$- and $y$-axis are converted from pixels to meters with the conversion values dx and dy. From the reconstructed images, $dx = dy = 0.5$ mm. As mentioned earlier, since there are no data available for the local gas velocities, we convert the $z$-axis or time axis into a length scale, where the averaged bubble velocity $\overline{v}_{bubble}$ is used, which is equal to the ratio of the superficial gas velocity and the time-averaged local gas hold-up (void fraction) ($v_{sup}/\alpha_{gas}$). It should be noted that the use of the $\overline{v}_{bubble}$ does not affect the
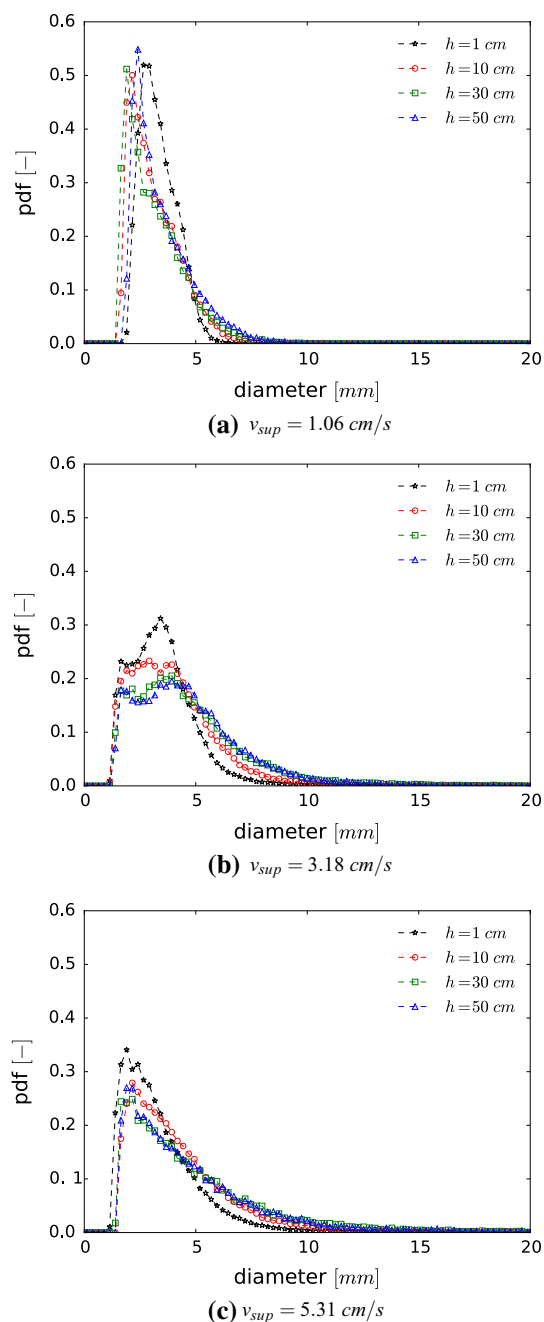


**Fig. 5** Bubble size distribution with superficial gas velocities of **a** 1.06, **b** 3.18 and **c** 5.31 cm/s at 4 different heights (1, 10, 30 and 50 cm)

positioning of the bubbles. The bubble centroids remain at their similar position within the hybrid-dimensional framework. Multiplication with the average bubble velocity, instead of the actual velocity, results in an averaged bubble size distribution, where fast rising bubbles are underestimated in size and slow rising bubbles overestimated in size.

For the lowest superficial gas velocity of 1.06 cm/s, the measured PDF near the sparger at $h = 1$ cm shows

that bubbles are little larger, highly affected by the injection pattern of the sparger than at other heights in the column, where the distribution is approximately similar. By increasing the gas velocity from 1.06 to 5.31 cm/s, shape changes are observed indicating a wider distribution of the bubble size. Since the shape of the PDFs remains similar throughout the column heights, it is argued that the effect of coalescence and breakup in the bubble column are quite low to nearly absent. The PDFs shape's changes from one superficial gas velocity to another are attributed to the increased inlet bubble size only. From the measurements, the number of bubbles per measurement duration decreases with increasing superficial gas velocity. For instance, the number of bubbles decreases from $\pm 30000$ bubbles for $v_{sup} = 1.06$ cm/s to $\pm 22,000$ bubbles for $v_{sup} = 3.18$ cm/s and to $\pm 14,000$ bubbles for $v_{sup} = 5.31$ cm/s. These values are similarly found at all measurement heights for the related superficial gas velocity. Together with shape similarity of the PDFs, an equilibrium of the number as well as size of the bubbles is observed.

## 4.2 Clustering within the bubble column

### 4.2.1 Effect of column height

Figure 6 illustrates the change in the volumetric distributions of the Voronoï diagrams with increasing height per superficial gas velocity. For the lowest superficial gas velocity of 1.06 cm/s, there are a large number of Voronoï cells with small volumes near the sparger at $h = 1$ cm compared with other heights in the column. This is expected since near the sparger bubbles' velocities are not developed yet. Near the injection point, the virtual mass force plays a significant role, causing the bubbles to be more packed than elsewhere higher in the column. Similar trends are observed at other gas velocities of 3.18 and 5.31 cm/s. The differences are, that at these larger velocities, there is a decreased number of bubbles with larger sizes, while the distribution at the heights 30 and 50 cm is approximately similar. This indicates that an equilibrium state has been reached, while at the lower gas velocity 1.06 cm/s, the distribution is not yet developed at the measured heights of 30 and 50 cm. Although the shapes of the bubble size distributions in Fig. 5 at larger velocities are approximately similar (e.g., from $h = 10$ cm to $h = 30$ cm at $v_{sup} = 5.31$ cm/s), Fig. 6 shows that the structures are not the same. It shows that the bubble size distributions develop faster and reach a steady state earlier than the structure itself.

To characterize the clustering behavior in the bubble column, the data of Fig. 6 are normalized (divided) with the average Voronoï volume and plotted together with the PDF of the randomly distributed Voronoï points. The random distribution is approximated with Eq. 1 (Ferenc and Néda
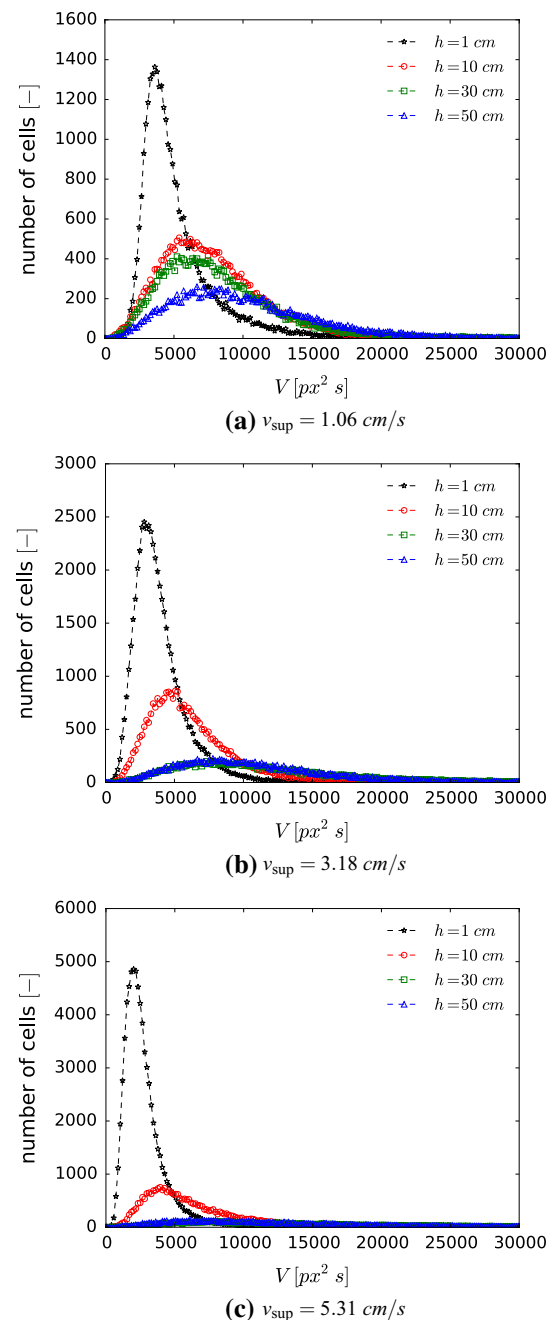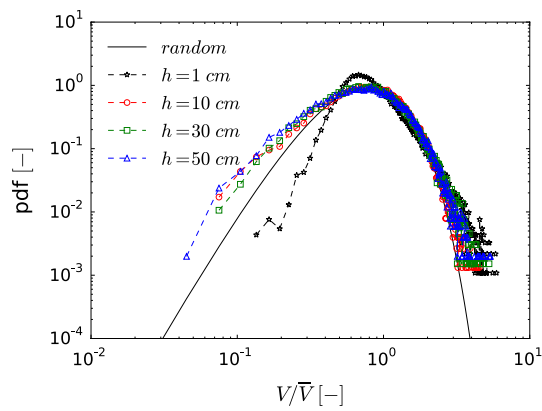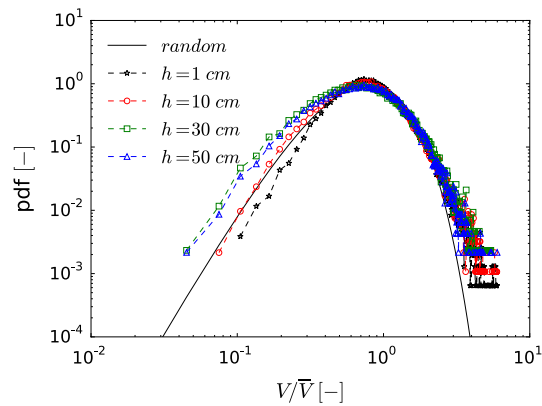


**(a)** $v_{sup} = 1.06$ cm/s

**(b)** $v_{sup} = 3.18$ cm/s

**(c)** $v_{sup} = 5.31$ cm/s

**Fig. 6** Size distribution of the Voronoï cell volumes at superficial gas velocities of 1.06, 3.18 and 5.31 cm/s for 4 different heights (1, 10, 30 and 50 cm)
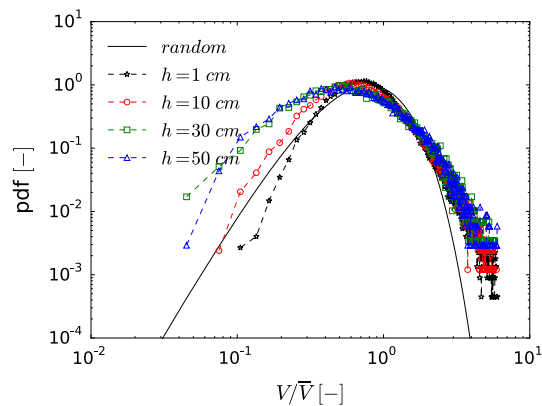
2007). The resulting plots are shown in Fig. 7. If there is no clustering in the bubble column, the measurement PDF should follow the shape of the random PDF. From the plots, for instance at a gas velocity of 1.06 cm/s (Fig. 7a), the measured PDFs deviate from the random PDF with an increased number of small and large Voronoï cells, indicating the presence of clustering, except for the measured PDF at the lowest height of 1 cm, where there is a smaller
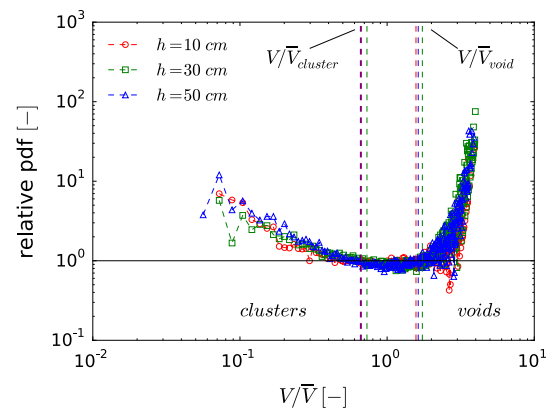
**Fig. 7** PDFs of normalized Voronoï volume ($V/\overline{V}$)
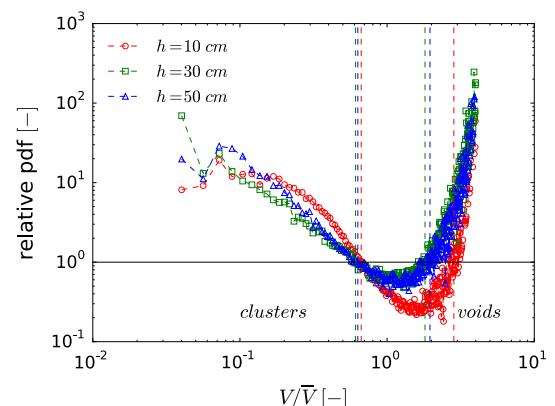


**Fig. 8** Relative PDFs of the Voronoï cells

amount of small Voronoï cells compared with the random PDF. The reason for this is that the measurement is taken near the sparger, where there is still a large influence of the ordered structure of the needle sparger. Higher in the column (10, 30 and 50 cm), the measured PDFs show an equal amount of small and large Voronoï cells. At higher gas velocities in Fig. 7a, b, an increase in small Voronoï cells is measured from $h = 1$ to 50 cm. From these plots, the increase in the superficial gas velocity results in an increase

in the averaged bubble size (from Fig. 5) and a wider structure of the experimental Voronoï PDF in comparison with the random PDF.

To visually emphasize the clusters, the relative PDFs between the experimental and random PDFs are illustrated in Fig. 8. The data of the measured PDF near the sparger are omitted here due to the large effect of the sparger on the structure of the bubbles. The two intersection points between the measured PDF and the line equal to 1 are
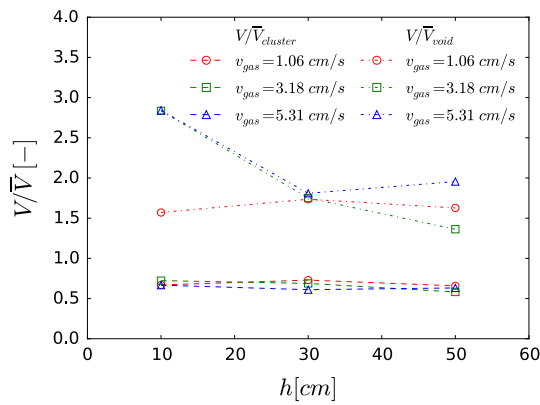
**Fig. 9** Cluster $V/\overline{V}_{cluster}$ and void $V/\overline{V}_{void}$ limits

considered to be the limits for clusters and voids. Cells with values smaller than $V/\overline{V}_{cluster}$ are considered as part of clusters and values larger than $V/\overline{V}_{void}$ are considered as part of voids. As mentioned earlier, the structure at a superficial gas velocity of 1.06 cm/s remains "steady", while at the higher gas velocities this so-called steady state is measured only above 30 cm height. The trend of both limits is illustrated in Fig. 9. The lower cluster limit $V/\overline{V}_{cluster}$ is approximately similar for all gas velocities at around 0.63 throughout the whole column. Contrarily, the upper limit $V/\overline{V}_{void}$ varies between 1.5 and 3.0 and shows no clear trend. A possible explanation for this behavior is coupled to the bubble size and velocity. At higher superficial gas velocities, bubble size and velocity are larger. These fast and bigger bubbles can create larger space or voidage in between bubbles, which is expressed in the variation of the void limit $V/\overline{V}_{void}$. Conversely, the smallest measurable bubble size is limited in all measurements by the accuracy of the experimental method. Hence, there isn't any smaller bubble available to be packed together within a single space, which relates to the steady value of the cluster limit $V/\overline{V}_{cluster}$.

### 4.2.2 Effect of superficial gas velocity

A comparison of the Voronoï size distribution of the different superficial gas velocities measured at a height of 50 cm is illustrated in Fig. 10. The decrease in the overall number of Voronoï cells in Fig. 10a is expected due to the lower number of larger-sized bubbles with increasing gas velocity. This comparison shows that due to the increased bubble size, there is a decrease in small Voronoï cells and in turn an increase in the large cells. Dividing by the averaged Voronoï cell size and normalizing the PDF (Fig. 10b) shows that there is actually an increasing amount of small Voronoï cells relative to the averaged volume. This result
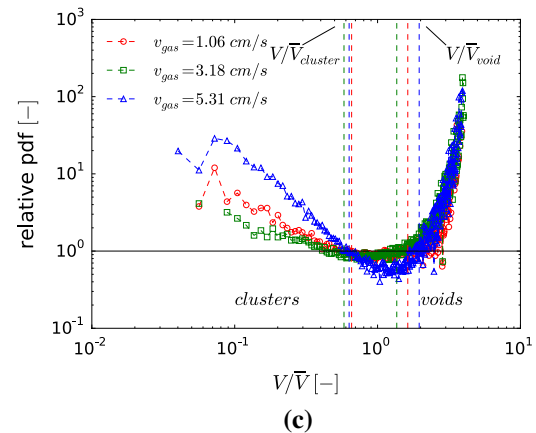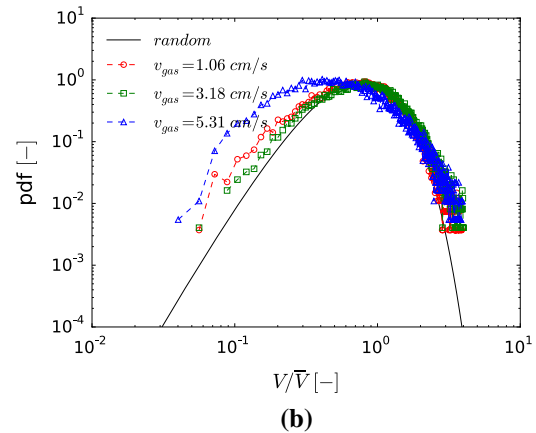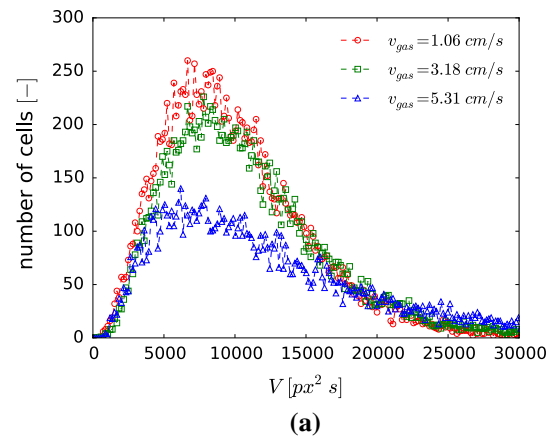


**Fig. 10** Distributions of Voronoï volumes at $h = 50$ cm with varying superficial gas velocity. **a** Size distribution, **b** Normalized PDF, **c** Relative PDF

indicates an increase in clustering within the bubble column at an increased gas velocity.

### 4.3 Effect of sparger

As an initial attempt to study the effect of the sparger design/configuration, additional experiments have been

**Fig. 11** Sparger configurations. **a** 115 needles with 0.40 mm inner diameter, **b** 24 needles with 0.80 mm inner diameter



(a)                                          (b)
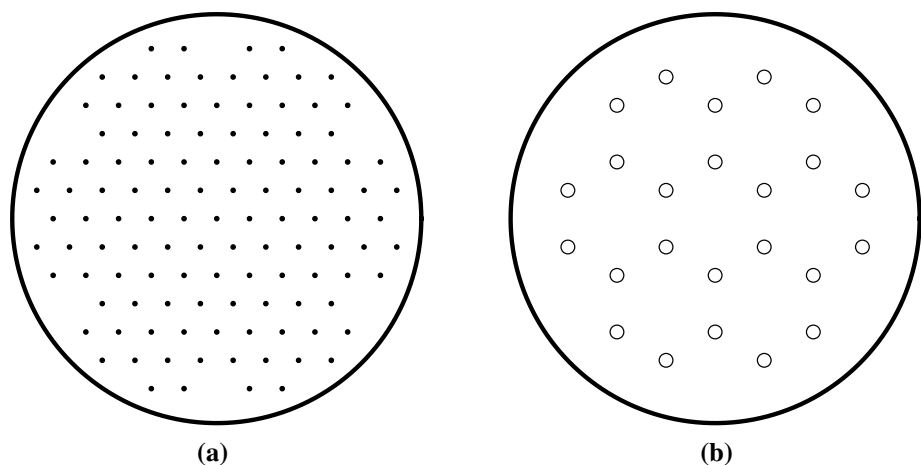
performed using different sparger configurations and inner needle diameters. Figure 11 illustrates the 115-needle sparger, which has been used in previous measurements, and a 24-needle sparger used in the current context. The measurement results of using the 24-needle sparger with an inner diameter of 0.8 mm are shown in Fig. 12 for the superficial gas velocity of 1.06 cm/s.

The differences are very large by comparing Figs. 5a and 12a. Due to the increased inner needle diameter, the total number of bubbles decreases from $\pm 30,000$ to $\pm 4000$. There is a wider bubble size distribution with a mean bubble diameter increasing from $\pm 3.5$ to $\pm 5.0$ mm. From the shape changes in the measurements with increasing height, it can be seen that coalescence and breakup of bubbles play a significant role in comparison with the results using the 115-needle sparger. Regarding the distribution of the Voronoï diagram given in Fig. 12b, starting from $h = 1$ cm to higher positions in the column, the peak of the Voronoï PDF decreases and the PDF widens, albeit slightly. This is also expressed in Fig. 12c, where the amount of small and large Voronoï cells increases with increasing height. In comparison with the results of the 115-needle sparger, it can be seen that the structuring of the bubbles using the 24-needle sparger, which has a wider bubble size distribution, does not change much over the height in the column. The cluster limits in Fig. 12d remains approximately 0.63 throughout the column and is equal to the experiments with 115 needles (Figs. 8 and 9). Contrary to latter mentioned experiments, there is a minor decrease in the void limit value, which decreases from 1.64 (at $h = 10$ cm) to 1.59 (at $h = 30$ cm) and finally to 1.41 (at $h = 50$ cm).

## 5 Conclusions

The Voronoï analysis of the ultrafast X-ray tomographic data is a convenient method to study clustering of bubbles in a bubble column. Experiments were performed with a 115-needle sparger operating at low superficial gas velocities. With increasing gas velocity, the bubble size distribution becomes wider, but remains similarly shaped throughout the whole column. From this observation, it is argued that the shape of the PDF is mainly determined by the inlet bubble size and the effect of coalescence and breakup of bubbles is very low or nearly absent.

While the shape of the bubble size distributions remains similar throughout the height of the column, the size distribution of the Voronoï cells develops from near the sparger to a steady state at approximately $h = 30$ cm. It has been observed that, with an increase in the superficial gas velocity, clustering of bubbles becomes more apparent. Evidently, by comparing the structure at a fixed height and an increasing gas velocity, the amount of bubbles as part of clusters and bubbles as part of voids increases with lesser bubbles in the column, but with a wider bubble size distribution. The presence of the increasing amount of bubbles as part of clusters at increasing gas velocities will have a significant impact on the heat and mass transfer processes. In the latter case, mass transfer is reduced, because the concentration of the dissolved gas in the liquid around a single gas bubble in a swarm depends not only on the mass transfer from the bubble itself, but also on the mass transfer from the other bubbles in the cluster.

By comparing the measured PDFs with the random PDF in all measurements, it is shown that, while the void limits $V/\overline{V}_{\text{void}}$ vary between 1.5 and 3.0, the cluster limits $V/\overline{V}_{\text{cluster}}$ remain approximately steady at 0.63 throughout the whole column. A possible explanation for the varying $V/\overline{V}_{\text{void}}$ value for different superficial gas velocities is due to the increased bubble size and velocity, while the $V/\overline{V}_{\text{cluster}}$ remains similar due to the measurable bubble size limit, which affects the possible maximum packing of bubbles. Furthermore, an initial attempt has shown that the sparger configuration plays a significant role on the bubble
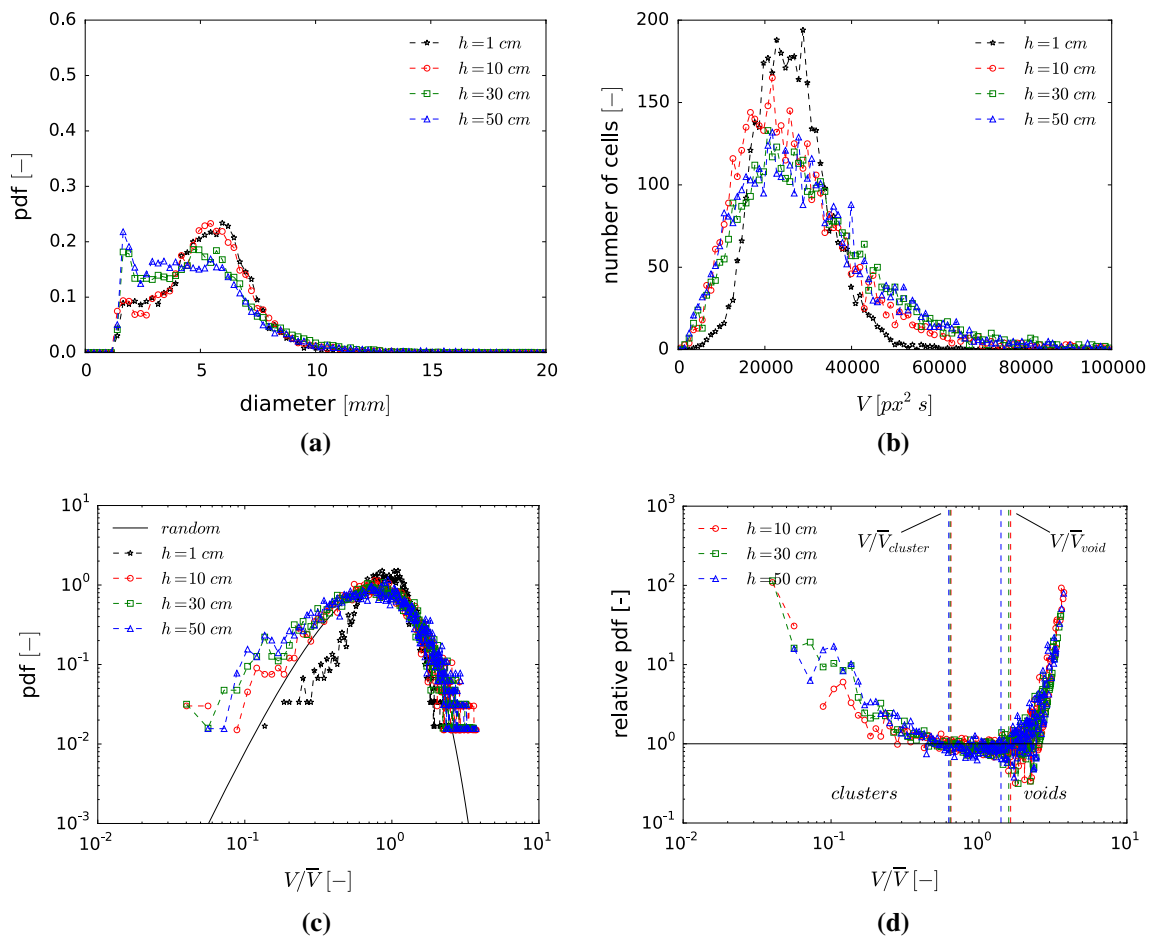
**Fig. 12** Measurements using the 24-needle sparger configuration. **a** Bubble size distribution, **b** Voronoï PDF, **c** Normalized PDF, **d** Relative PDF

size distribution as well as on the structuring of bubbles. It can be seen that changes in the bubble structure over the height of the column are smaller for a wider bubble size distribution.

# References

Acuña CA, Finch JA (2010) Tracking velocity of multiple bubbles in a swarm. Int J Miner Process 94:147–158. doi:10.1016/j.minpro.2010.02.001

Aliseda A, Cartellier A, Hainaux F, Lasheras JC (2002) Effect of preferential concentration on the settling velocity of heavy particles in homogeneous isotropic turbulence. J Fluid Mech 468:77–105. doi:10.1017/S0022112002001593

Bunner B, Tryggvason G (2002) Dynamics of homogeneous bubbly flows Part 1. Rise velocity and microstructure of the bubbles. J Fluid Mech 466:17–52. doi:10.1017/S0022112002001179

Bunner B, Tryggvason G (2003) Effect of bubble deformation on the properties of bubbly flows. J Fluid Mech 495:77–118. doi:10.1017/S0022112002001180

Esmaeeli A, Tryggvason G (1998) Direct numerical simulations of bubbly flows. Part 1. Low Reynolds number arrays. J Fluid Mech 377:313–345. doi:10.1017/S0022112098003176

Esmaeeli A, Tryggvason G (1999) Direct numerical Simulations of bubbly flows Part 2. Moderate Reynolds number arrays. J Fluid Mech 385:325–358. doi:10.1017/S0022112099004310

Ferenc JS, Néda Z (2007) On the size distribution of Poisson Voronoï cells. Phys A 385:518–526. doi:10.1016/j.physa.2007.07.063

Ferreira A, Pereira G, Teixeira JA, Rocha F (2008) Statistical tool combined with image analysis to characterize hydrodynamics and mass transfer in a bubble column. Chem Eng J 180:216–228. doi:10.1016/j.cej.2011.09.117

Fischer F, Hampel U (2010) Ultra fast electron beam X-ray computed tomography for two-phase flow measurement. Nucl Eng Des 240:2254–2259. doi:10.1016/j.nucengdes.2009.11.016

Fischer F, Hoppe D, Schleicher E, Mattausch G, Flaske H, Bartel R, Hampel U (2008) An ultra fast electron beam

X-ray tomography scanner. Meas Sci Technol 19:094002. doi:10.1088/0957-0233/19/9/094002

Hampel U, Barthel F, Bieberle M, Schubert M, Schleicher E (2012) Multiphase flow investigations with ultrafast electron beam X-ray tomography. AIP Conference Proceedings 1428:167

Koch DL (1993) Hydrodynamic diffusion in dilute sedimenting suspensions at moderate Reynolds numbers. Phys Fluids A 5:1141–1155

Lamb H (1932) Hydrodynamics. Dover, New York

Martinez Mercado J, Chehata Gomez D, van Gils D, Sun C, Lohse D (2010) On bubble clustering and energy spectra in pseudo-turbulence. J Fluid Mech 650:287–306. doi:10.1017/S0022112009993570

Martinez Mercado J, Prakash VN, Tagawa Y, Sun C, Lohse D (2012) Lagrangian statistics of light particles in turbulence. Phys Fluids 24:055106. doi:10.1063/1.4719148

Mazzitelli IM, Lohse D (2009) Evolution of energy in flow driven by rising bubbles. Phys Rev E 79:066317. doi:10.1103/PhysRevE.79.066317

Monchaux R, Bourgoin M, Cartellier A (2010) Preferential concentration of heavy particles: A Voronoï analysis. Phys Fluids 22:103304. doi:10.1063/1.3489987

Monchaux R, Bourgoin M, Cartellier A (2012) Analyzing preferential concentration and clustering of inertial particles in turbulence. Int J Multiph Flow 40:1–18. doi:10.1016/j.ijmultiphaseflow.2011.12.001

Okabe A, Boots B, Sugihara K, Chiu SN (2000) Spatial tessellations - concepts and applications of Voronoi diagrams. Wiley: Hoboken. doi:10.1002/9780470317013

Risso F, Ellingsen K (2002) Velocity fluctuations in a homogeneous dilute dispersion of high-Reynolds-number rising bubbles. J Fluid Mech 453:395–410. doi:10.1017/S0022112001006930

Sangani AS, Didwania AK (1993) Dynamic simulations of flows of bubbly liquids at large Reynolds numbers. J Fluid Mech 250:307–337. doi:10.1017/S0022112093001478

Santarelli C, Fröhlich J (2013) On the pair correlation function in a bubble swarm. Kerntechnik 78:50–51

Smereka P (1993) On the motion of bubbles in a periodic box. J Fluid Mech 254:79–112. doi:10.1017/S0022112093002046

Smolianski A, Haario H, Luukka P (2008) Numerical study of dynamics of single bubbles and bubble swarms. Appl Math Model 32:641–659. doi:10.1016/j.apm.2007.01.004

Tagawa Y, Martinez Mercado J, Vivek NP, Calzavarini E, Sun C, Lohse D (2012) Three-dimensional Lagrangian Voronoï analysis for clustering of particles and bubbles in turbulence. J Fluid Mech 693:201–215. doi:10.1017/jfm.2011.510

Yianatos JB, Finch JA, Dobby GS, Xu M (1988) Bubble size estimation in a bubble swarm. J Colloid Interface Sci 126: doi:10.1016/0021-9797(88)90096-3

Zenit R, Koch DL, Sangani AS (2001) Measurements of the average properties of a suspension of bubbles rising in a vertical channel. J Fluid Mech 429:307–342. doi:10.1017/S0022112000002743